Hindawi
Advances in High Energy Physics
Volume 2018, Article ID 2547358, 11 pages
https://doi.org/10.1155/2018/2547358

Research Article

Degeneracy Resolution Capabilities of NOνA and DUNE in the Presence of Light Sterile Neutrino

Akshay Chatla[1] **Sahithi Rudrabhatla**[2] **and Bindu A. Bambah**[1]

[1] *School of Physics, University of Hyderabad, Hyderabad 500046, India*
[2] *Department of Physics, University of Illinois at Chicago, Chicago, IL 60607, USA*

Correspondence should be addressed to Akshay Chatla; chatlaakshay@gmail.com

Received 10 April 2018; Accepted 15 August 2018; Published 6 September 2018

Academic Editor: Hiroyasu Ejiri

We investigate the implications of a sterile neutrino on the physics potential of the proposed experiment DUNE and future runs of NOνA using latest NOνA results. Using combined analysis of the disappearance and appearance data, NOνA reported preferred solutions at normal hierarchy (NH) with two degenerate best-fit points: one in the lower octant (LO) and $\delta_{13} = 1.48\pi$ and the other in higher octant (HO) and $\delta_{13} = 0.74\pi$. Another solution of inverted hierarchy (IH), which is 0.46σ away from best fit, was also reported. We discuss chances of resolving these degeneracies in the presence of sterile neutrino.

1. Introduction

Sterile neutrinos are hypothetical particles that do not interact via any of the fundamental interactions other than gravity. The term sterile is used to distinguish them from active neutrinos, which are charged under weak interaction. The theoretical motivation for sterile neutrino explains the active neutrino mass after spontaneous symmetry breaking, by adding a gauge singlet term (sterile neutrino) to the Lagrangian under $SU(3)_c \otimes SU(2)_L \otimes U(1)_r$ where the Dirac term appears through the Higgs mechanism, and Majorana mass term is a gauge singlet and hence appears as a bare mass term [1]. The diagonalization of the mass matrix gives masses to all neutrinos due to the See-Saw mechanism.

Some experimental anomalies also point towards the existence of sterile neutrinos. Liquid Scintillator Neutrino Detector (LSND) detected $\overline{\nu}_\mu \longrightarrow \overline{\nu}_e$ transitions indicating $\Delta m^2 \approx 1eV^2$ which is inconsistent with $\Delta m^2_{32}, \Delta m^2_{21}$ (LSND anomaly) [2]. Measurement of the width of Z boson by LEP gave number of active neutrinos to be 2.984 ± 0.008 [3]. Thus the new neutrino introduced to explain the anomaly has to be a sterile neutrino. MiniBooNE, designed to verify the LSND anomaly, observed an unexplained excess of events in low-energy region of $\overline{\nu}_e, \nu_e$ spectra, consistent with LSND [4]. SAGE and GALLEX observed lower event rate than expected, explained by the oscillations of ν_e due to $\Delta m^2 \geq 1eV^2$(Gallium anomaly) [5–7]. Recent precise predictions of reactor antineutrino flux have increased the expected flux by 3% over old predictions. With the new flux evaluation, the ratio of observed and predicted flux deviates at 98.6% C.L (Confidence level) from unity; this is called "reactor antineutrino anomaly" [8]. This anomaly can also be explained using sterile neutrino model.

Short-baseline (SBL) experiments are running to search for sterile neutrinos. SBL experiments are the best place to look for sterile neutrino, as they are sensitive to new expected mass-squared splitting $\Delta \mathrm{m}^2 \simeq 1\mathrm{eV}^2$. However, SBL experiments cannot study all the properties of sterile neutrinos, mainly new CP phases introduced by sterile neutrino models. These new CP phases need long distances to become measurable [9, 10] and thus can be measured using long baseline (LBL) experiments. With the discovery of relatively large value for θ_{13} by Daya Bay [11], the sensitivity of LBL experiments towards neutrino mass hierarchy and CP phases increased significantly. In this context, some phenomenological studies regarding the sensitivity of LBL experiments can be found in recent works [12–16]. Using recent global fits of oscillation parameters in the 3+1 scenario

[17], current LBL experiments can extract two out of three CP phases (one of them being standard δ_{13}) [10]. The phenomenological studies of LBL experiments in presence of sterile neutrino is studied by several groups [18–23]. Now, the sensitivity of LBL experiments towards their original goals decreases due to sterile neutrinos. It is seen in case of the CPV measurement; new CP phases will decrease the sensitivity towards standard CP phase (δ_{13}). This will reduce degeneracy resolution capacities of LBL experiments. In this paper, we study hierarchy-θ_{23}-δ_{13} degeneracies using contours in θ_{23}-δ_{13} plane and how they are affected by the introduction of sterile neutrinos. We attempt to find the extent to which these degeneracies can be resolved in future runs of NOνA and DUNE.

The outline of the paper is as follows. In Section 2, we present the experimental specifications of NOνA and DUNE used in our simulation. We introduce the effect of sterile neutrino on parameter degeneracies resolution in Section 3. Section 4 contains the discussion about the degeneracy resolving capacities of future runs of NOνA and DUNE assuming latest NOνA results—NH- (normal hierarchy-) LO (lower octant); NH-HO (higher octant); and IH- (inverted hierarchy-) HO—as true solutions for both 3 and 3+1 models. Finally, Section 5 contains concluding comments on our results.

2. Experiment Specifications

We used GLoBES (General Long Baseline Experiment Simulator) [24, 25] to simulate the data for different LBL experiments including NOνA and DUNE. The neutrino oscillation probabilities for the 3+1 model are calculated using the new physics engine available from [26].

NOνA [27, 28] is an LBL experiment which started its full operation from October 2014. NOνA has two detectors: the near detector is located at Fermilab (300 ton, 1 km from NuMI beam target) while the far detector (14 Kt) is located at Northern Minnesota 14.6 mrad off the NuMI beam axis at 810 km from NuMI beam target, justifying “off-axis” in the name. This off-axis orientation gives us a narrow beam of flux, peak at 2 GeV [29]. For simulations, we used NOνA setup from [30]. We used the full projected exposure of 3.6×10^{21} p.o.t (protons on target) expected after six years of runtime at 700 kW beam power. Assuming the same runtime for neutrino and antineutrino modes, we get 1.8×10^{21} p.o.t for each mode. Following [31] we considered 5% normalization error for the signal and 10% error for the background for appearance and disappearance channels.

DUNE (Deep Underground Neutrino Experiment) [32, 33] is the next generation LBL experiment. Long Base Neutrino Facility (LBNF) of Fermilab is the source for DUNE. Near detector of DUNE will be at Fermilab. Liquid Argon detector of 40 kt to be constructed at Sanford Underground Research Facility, situated 1300 km from the beam target, will act as the far detector. DUNE uses the same source as of NOνA; we will observe beam flux peak at 2.5GeV. We used DUNE setup give in [34] for our simulations. Since DUNE is still in its early stages, we used simplified systematic treatment, i.e., 5% normalization error on signal and 10% error on the background for both appearance and disappearance spectra. We give experimental details described above in tabular form in Tables 1 and 2.

Oscillation parameters are estimated from the data by comparing observed and predicted ν_e and ν_μ interaction rates and energy spectra. GLoBES calculates event rates of neutrinos for energy bins taking systematic errors, detector resolutions, MSW effect due to earth's crust, etc. into account. The event rates generated for true and test values are used to plot χ^2 contours. GLoBES uses its inbuilt algorithm to calculate χ^2 values numerically considering parameter correlations as well as systematic errors. In our calculations we used χ^2 as

$$\chi^2 = \sum_{\mathrm{i}=1}^{\#\mathrm{ofbins}} \sum_{\mathrm{E_n}=\mathrm{E_1},\mathrm{E_2}\ldots} \frac{\left(\mathrm{O}_{\mathrm{E_n},\mathrm{i}} - \left(1 + \mathrm{a_F} + \mathrm{a}_{\mathrm{E_n}}\right)\mathrm{T}_{\mathrm{E},\mathrm{i}}\right)^2}{\mathrm{O}_{\mathrm{E_n},\mathrm{i}}} + \frac{\mathrm{a_F^2}}{\sigma_\mathrm{F}^2} + \frac{\mathrm{a}_{\mathrm{E_n}}^2}{\sigma_{\mathrm{E_n}}^2} \quad (1)$$

where $\mathrm{O}_{\mathrm{E_1},\mathrm{i}}, \mathrm{O}_{\mathrm{E_2},\mathrm{i}} \ldots$ are the event rates for the i^{th} bin in the detectors of different experiments, calculated for true values of oscillation parameters; $\mathrm{T}_{\mathrm{E_n},\mathrm{i}}$ are the expected event rates for the i^{th} bin in the detectors of different experiments for the test parameter values; $\mathrm{a_F}, \mathrm{a}_{\mathrm{E_n}}$ are the uncertainties associated with the flux and detector mass; and σ_F, σ_{E_n} are the respective associated standard deviations. The calculated χ^2 function gives the confidence level in which tested oscillation parameter values can be ruled out with referenced data. It provides an excellent preliminary evaluation model to estimate the experiment performance.

3. Theory

In a 3+1 sterile neutrino model, the flavour and mass eigenstates are connected through a 4×4 mixing matrix. A convenient parametrization of the mixing matrix is [36]

$$U = R_{34}\widetilde{R_{24}}\widetilde{R_{14}}R_{23}\widetilde{R_{13}}R_{12}. \quad (2)$$

Here R_{ij} and $\widetilde{R_{ij}}$ represent real and complex 4×4 rotation in the plane containing the 2×2 subblock in (i, j) subblock

$$R_{ij}^{2\times2} = \begin{pmatrix} c_{ij} & s_{ij} \\ -s_{ij} & c_{ij} \end{pmatrix} \qquad \widetilde{R_{ij}}^{2\times2} = \begin{pmatrix} c_{ij} & \widetilde{s_{ij}} \\ -\widetilde{s_{ij}}^{*} & c_{ij} \end{pmatrix} \quad (3)$$

where, $c_{ij} = \cos\theta_{ij}$, $s_{ij} = \sin\theta_{ij}$, $\widetilde{s_{ij}} = s_{ij}e^{-i\delta_{ij}}$, and δ_{ij} are the CP phases.

There are three mass-squared difference terms in 3+1 model: $\Delta\mathrm{m}_{21}^2$(solar)$\simeq 7.5 \times 10^{-5}\mathrm{eV}^2$, $\Delta\mathrm{m}_{31}^2$ (atmospheric)$\simeq 2.4 \times 10^{-3}\mathrm{eV}^2$, and $\Delta\mathrm{m}_{41}^2$(sterile)$\simeq 1\mathrm{eV}^2$. The mass-squared difference term towards which the experiment is sensitive depends on L/E of the experiment. Since SBL experiments have a very small L/E, $\sin^2(\Delta m_{ij}^2 L/4E) \simeq 0$ for $\Delta\mathrm{m}_{21}^2$ and $\Delta\mathrm{m}_{31}^2$. $\Delta\mathrm{m}_{41}^2$ term survives. Hence, SBL experiments

TABLE 1: Details of experiments.

Name of Exp	NOνA	DUNE
Location	Minnesota	South Dakota
POT(yr^{-1})	6.0x10^{20}	1.1x10^{21}
Baseline(Far/Near)	812 km/1km	1300 km/500 m
Target mass(Far/Near)	14 kt/290 t	40 kt/8 t
Exposure(years)	6	10
Detector type	Tracking Calorimeters	LArTPCs

TABLE 2: Systematic errors associated with NOνA and DUNE.

Name of Exp	Rule	Normalization error	
		signal(%)	background(%)
NOνA	ν_e appearance	5	10
	ν_μ disappearance	2	10
	$\overline{\nu}_e$ appearance	5	10
	$\overline{\nu}_\mu$ disappearance	2	10
DUNE	ν_e appearance	5	10
	ν_μ disappearance	5	10
	$\overline{\nu}_e$ appearance	5	10
	$\overline{\nu}_\mu$ disappearance	5	10

depend only on sterile mixing angles and are insensitive to the CP phases. The oscillation probability, $P_{\mu e}$ for LBL experiments in 3+1 model, after averaging Δm^2_{41} oscillations and neglecting MSW effects, [37] is expressed as sum of the four terms

$$P^{4\nu}_{\mu e} \simeq P_1 + P_2(\delta_{13}) + P_3(\delta_{14}-\delta_{24}) + P_4(\delta_{13}-(\delta_{14}-\delta_{24})). \quad (4)$$

These terms can be approximately expressed as follows:

$$P_1 = \frac{1}{2}\sin^2 2\theta^{4\nu}_{\mu e} + \left[a^2\sin^2 2\theta^{3\nu}_{\mu e} - \frac{1}{4}\sin^2 2\theta_{13}\sin^2 2\theta^{4\nu}_{\mu e}\right] \cdot \sin^2\Delta_{31} + \left[a^2 b^2 - \frac{1}{4}\sin^2 2\theta_{12} \cdot \left(\cos^4\theta_{13}\sin^2 2\theta^{4\nu}_{\mu e} + a^2\sin^2 2\theta^{3\nu}_{\mu e}\right)\right]\sin^2\Delta_{21}, \quad (5)$$

$$P_2(\delta_{13}) = a^2 b\sin 2\theta^{3\nu}_{\mu e}\left(\cos 2\theta_{12}\cos\delta_{13}\sin^2\Delta_{21} - \frac{1}{2} \cdot \sin\delta_{13}\sin 2\Delta_{21}\right), \quad (6)$$

$$P_3(\delta_{14}-\delta_{24}) = ab\sin 2\theta^{4\nu}_{\mu e}\cos^2\theta_{13}\left[\cos 2\theta_{12} \cdot \cos(\delta_{14}-\delta_{24})\sin^2\Delta_{21} - \frac{1}{2}\sin(\delta_{14}-\delta_{24}) \cdot \sin 2\Delta_{21}\right], \quad (7)$$

$$P_4(\delta_{13}-(\delta_{14}-\delta_{24})) = a\sin 2\theta^{3\nu}_{\mu e}\sin 2\theta^{4\nu}_{\mu e}\left[\cos 2\theta_{13} \cdot \cos(\delta_{13}-(\delta_{14}-\delta_{24}))\sin^2\Delta_{31} + \frac{1}{2} \cdot \sin(\delta_{13}-(\delta_{14}-\delta_{24}))\sin 2\Delta_{31} - \frac{1}{4}\sin^2 2\theta_{12} \cdot \cos^2\theta_{13}\cos(\delta_{13}-(\delta_{14}-\delta_{24}))\sin^2\Delta_{21}\right], \quad (8)$$

with the parameters defined as

$$\Delta_{ij} \equiv \frac{\Delta m^2_{ij} L}{4E}, \text{a function of baseline (L) and neutrino energy (E)}$$
$$a = \cos\theta_{14}\cos\theta_{24},$$
$$b = \cos\theta_{13}\cos\theta_{23}\sin 2\theta_{12},$$
$$\sin 2\theta^{3\nu}_{\mu e} = \sin 2\theta_{13}\sin\theta_{23},$$
$$\sin 2\theta^{4\nu}_{\mu e} = \sin 2\theta_{14}\sin\theta_{24}. \quad (9)$$

The CP phases introduced due to sterile neutrinos persist in the $P_{\mu e}$ even after averaging out Δm^2_{41} lead oscillations. Last two terms of (4) give the sterile CP phase dependence terms. $P_3(\delta_{14}-\delta_{24})$ depends on the sterile CP phases δ_{14} and δ_{24}, while P_4 depends on a combination of δ_{13} and $\delta_{14}-\delta_{24}$. Thus, we expect LBL experiments to be sensitive to sterile phases. We note that the probability $P_{\mu e}$ is independent θ_{34}. One can see that θ_{34} will effect $P_{\mu e}$ if we consider earth mass effects. Since matter effects are relatively small for

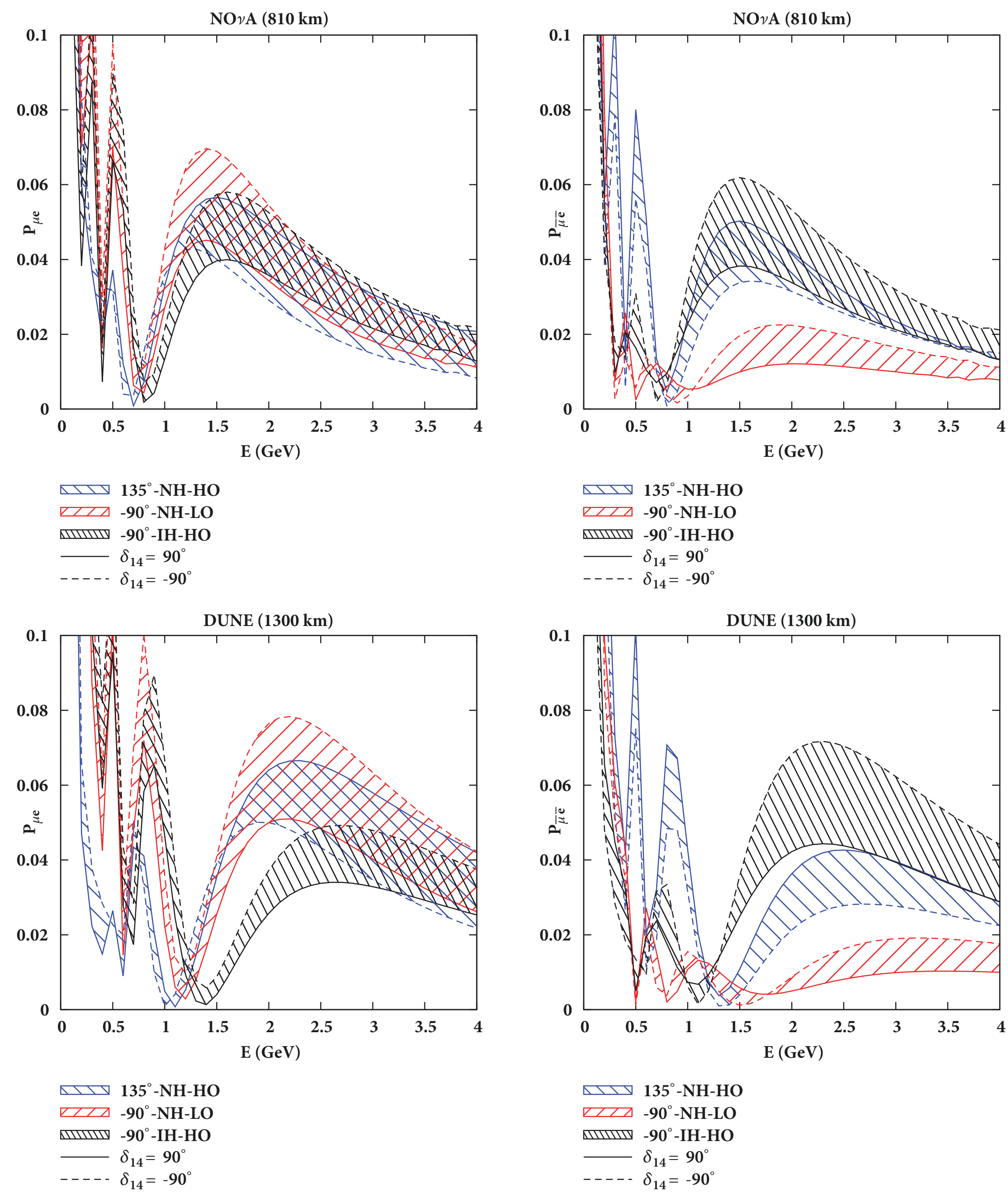

Figure 1: The oscillation probability $P_{\mu e}$ as a function of energy. The top (bottom) panel is NOνA (DUNE). The bands correspond to different values of δ_{14}, ranging from -180° to 180° when $\delta_{24} = 0°$. Inside each band, the probability for $\delta_{14} = 90°$ ($\delta_{14} = -90°$) case is shown as the solid (dashed) line. The left (right) panel corresponds to neutrinos (antineutrinos).

NOνA and DUNE, their sensitivity towards θ_{34} is negligible. The amplitudes of atmospheric-sterile interference term (8) and solar-atmospheric interference term (6) are of the same order. This new interference term reduces the sensitivity of experiments to the standard CP phase (δ_{13}).

In Figure 1, we plot the oscillation probability ($P_{\mu e}$) as a function of energy while varying δ_{14} (-180° to 180°) and keeping $\delta_{24} = 0$ for the three best-fit values of latest NOνA results [35], i.e., NH-LO-1.48π[δ_{13}], NH-HO-0.74π, and IH-HO-1.48π, where HO implies $\sin^2\theta_{23} = 0.62$ and LO implies

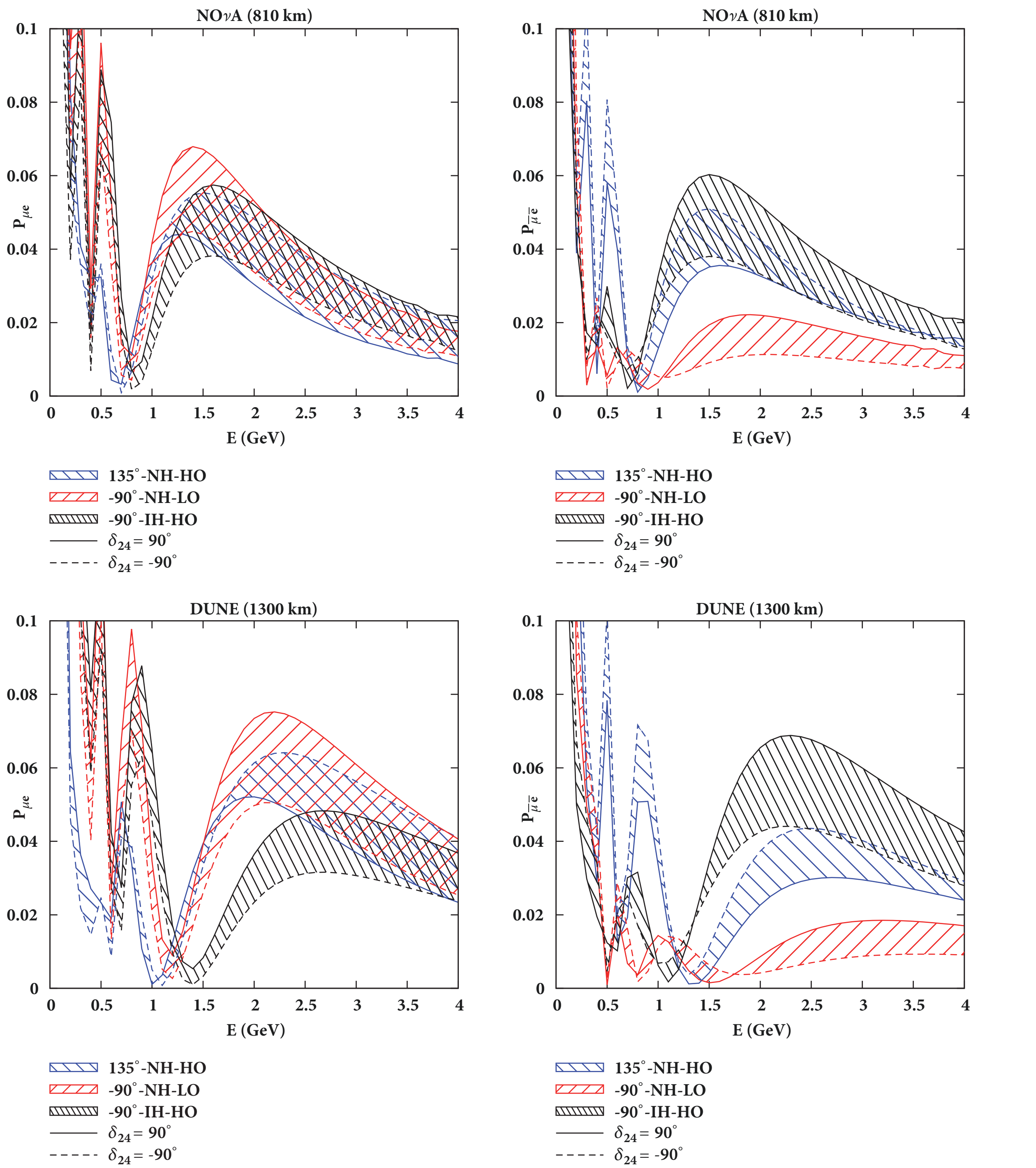

FIGURE 2: The oscillation probability $P_{\mu e}$ as a function of energy. The top (bottom) panel is NOνA (DUNE). The bands correspond to different values of δ_{24}, ranging from -180° to 180° when $\delta_{14} = 0°$. Inside each band, the probability for $\delta_{24} = 90°$ ($\delta_{24} = -90°$) case is shown as solid (dashed) line. The left (right) panel is for neutrinos (antineutrinos).

$\sin^2\theta_{23} = 0.40$. For the flux peak of NOνA, $E \approx 2$GeV, we observe a degeneracy between all best-fit values due to the presence of δ_{14} band for neutrino case, while only NH-HO and IH-HO bands overlap in antineutrino case. We see that δ_{14} phase decreases both octant and hierarchy resolution capacity for neutrino case and only mass hierarchy resolution capacity for antineutrino case. The second row plots $P_{\mu e}$ for DUNE at baseline 1300 km. We observe smaller overlap between bands compared to NOνA. Thus, the decrease of degeneracy resolution capacity for DUNE is less than NOνA. Similarly we plot $P_{\mu e}$ while varying δ_{24}(-180° to 180°) in Figure 2 and keeping $\delta_{14} = 0°$. We see that δ_{24} has similar

Table 3: Oscillation parameters considered in numerical analysis. The $\sin^2\theta_{23}$ and δ_{13} are taken from latest NOνA results [35].

Parameter	True value	Marginalization Range
$\sin^2\theta_{12}$	0.304	Not Marginalized
$\sin^2 2\theta_{13}$	0.085	[0.075,0.095]
$\sin^2\theta_{23}$	0.623(HO),0.404(LO)	[0.32,0.67]
$\sin^2\theta_{14}$	0.025	Not Marginalized
$\sin^2\theta_{24}$	0.025	Not Marginalized
$\sin^2\theta_{34}$	0.025	Not Marginalized
δ_{13}	135(NH-HO),-90(NH-LO,IH)	[-180,180]
δ_{14}	[-180,180]	[-180,180]
δ_{24}	[-180,180]	[-180,180]
Δm^2_{21}	7.50×10^{-5} eV^2	Not Marginalized
Δm^2_{31}(NH)	2.40×10^{-3} eV^2	Not Marginalized
Δm^2_{31}(IH)	-2.33×10^{-3} eV^2	Not Marginalized
Δm^2_{41}	1 eV^2	Not Marginalized

effect to that of δ_{14}; the only change is reversal of δ_{24} band extrema; i.e., $\delta_{24} = -90^\circ$ gives the same result as $\delta_{14} = 90^\circ$ and vice versa. This can be explained using (4) in which we see δ_{14} and δ_{24} are always together with opposite signs. Overall from the probability plots, we observe that the addition of new CP phases decreases octant and mass hierarchy resolution capacities.

In the next section, we explore how parameter degeneracies are affected in the 3+1 model and the extent to which these degeneracies can be resolved in future runs of NOνA and DUNE.

4. Results for NOνA and DUNE

We explore allowed regions in $\sin^2\theta_{23}$-δ_{cp} plane from NOνA and DUNE simulation data with different runtimes, considering latest NOνA results as true values. Using combined analysis of the disappearance and appearance data, NOνA reported preferred solutions [35] at normal hierarchy (NH) with two degenerate best-fit points: one in the lower octant (LO) and $\delta_{cp} = 1.48\pi$ and the other in higher octant (HO) and $\delta_{cp} = 0.74\pi$. Another solution of inverted hierarchy (IH), 0.46σ away from best fit, is also reported. Table 3 shows true values of oscillation parameters and their marginalization ranges we used in our simulation. By studying the allowed regions, we understand the extent to which future runs of NOνA and DUNE will resolve these degeneracies, if the best-fit values are true values.

In the first row of Figure 3, we show allowed areas for NOνA[3+$\overline{0}$]. In first plot of first row, we show 90% C.L allowed regions for true values of $\delta_{13} = 135^\circ$ and $\theta_{23} = 52^\circ$ and normal hierarchy. We plot test values for both NH and IH, of 3 and 3+1 neutrino models. We observe that introducing sterile neutrino largely decreases the precision of θ_{23}. The WO-RH region, for 3ν case confined between 45° and -180° of δ_{13}, confines the whole δ_{13} region for 4ν case. The WH-RO region of 3ν case doubles, covering the entire region of δ_{13} for 4ν case. The 3+1 model also introduces a small WH-WO region, which was absent in 3ν model. In the second plot of first row (true value $\delta_{13} = -90^\circ$, $\theta_{23} = 40^\circ$ and normal hierarchy), for the 3ν case, we see RH-RO region excluding 45° to 150° of δ_{13}, while RH-WO region covers the whole of the δ_{13} region. In 3+1 model, both RH-RO and RH-WO regions cover the whole of the δ_{13} region. WH-RO solution occupies a small region for 3ν case, covering half of δ_{13} region for 4ν case. WH-WO region covers the whole of the δ_{13} region for 4ν case. In the third plot of first row, true values are taken as $\delta_{13} = -90^\circ$, $\theta_{23} = 52^\circ$ and inverted hierarchy. The RH-RO region covers the entire range of δ_{13} for both 3ν and 4ν case, whereas RH-WO region almost doubles from 3ν case to 4ν case. A small range of δ_{13} excluded from WH-RO for 3ν case is covered in 4ν case. WH-WO region of 3ν case excludes 60° to 150° of δ_{13} while full δ_{13} range is covered for 4ν case.

In the second row of the figure, we plot allowed regions for NOνA[3+$\overline{1}$]. We take true values as best-fit points obtained by NOνA. We observe an increase in precision of parameter measurement, due to an increase in statistics, from added 1 yr of antineutrino run. In the first plot of the second row, the RH-RO octant region covers entire δ_{13} range for both 3ν and 4ν case. RH-WO region includes -180° to 45° of δ_{13} for 3ν case, while the whole range of δ_{13} is covered in 4ν case. A slight increase in the area of WH-RO is observed form 3ν to 4ν case. 4ν introduces WH-WO region which was resolved for 3ν case. In the second plot, RH-RO region allows full range of δ_{13} for 4ν case, while it was restricted to lower half of CP range in 3ν case. We see that WH-RO solution, which was resolved in 3ν case, is reintroduced in 4ν case. We also see a slight increase in the size of WH-WO solution from 3ν to 4ν. In third plot, RH-RO region covers the whole CP range for 4ν while 35° to 125° of δ_{13} are excluded in 3ν case. The almost resolved RH-WO solution for 3ν doubles for 4ν case. WH-RO and WH-WO cover the entire region of δ_{13} for 4ν case.

In the third row, we show allowed regions for NOνA[3+$\overline{3}$]. In the first plot, it can be seen that small area of RH-WO in case of 3ν now covers the whole of δ_{13} region for 4ν case. While the 3ν case has WH-Wδ_{13} degeneracy, 4ν case introduces equal sized WH-WO-Wδ_{13} degeneracy. In second plot, for 3ν case most of δ_{13} values above 0° are excluded, but

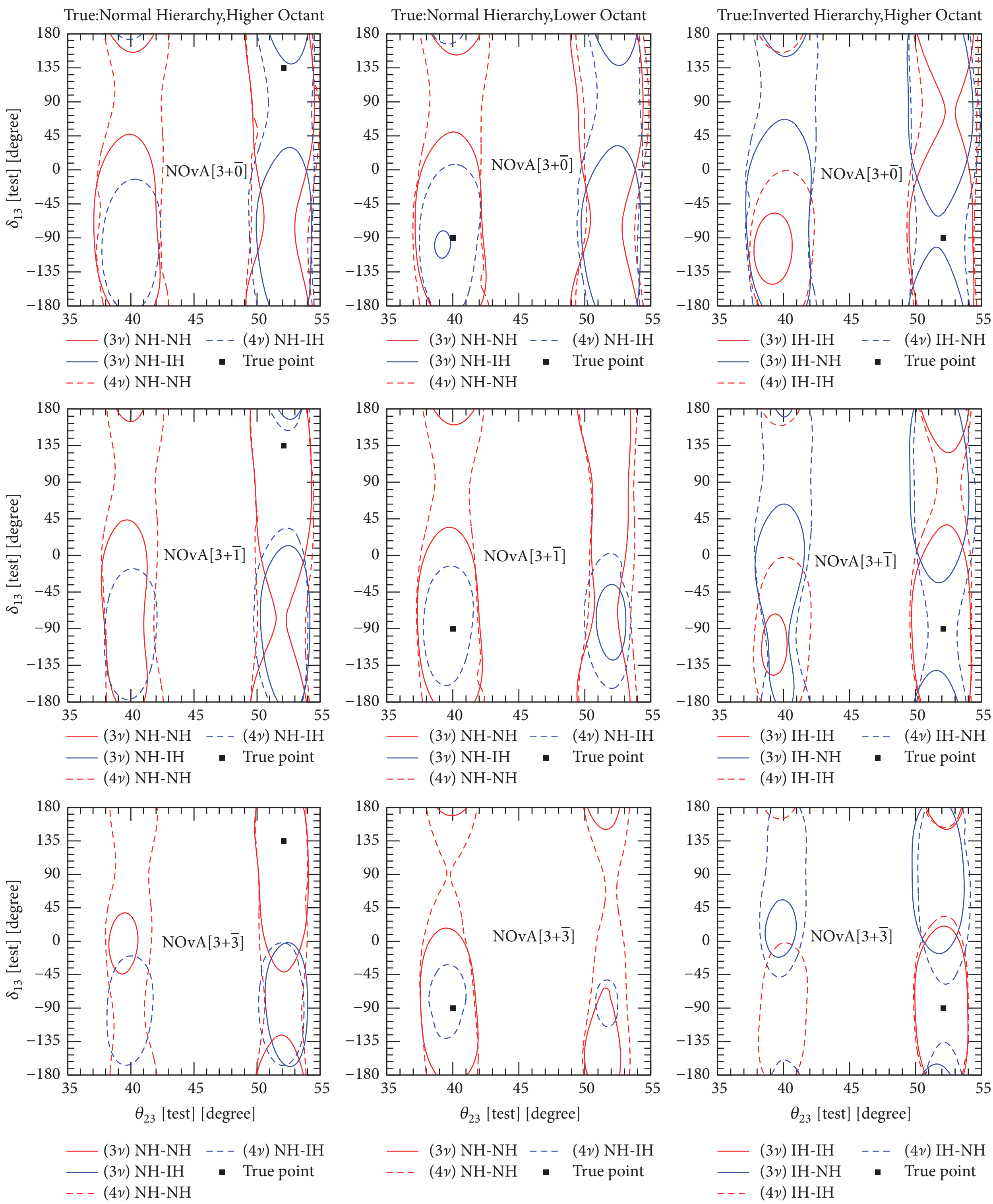

FIGURE 3: Contour plots of allowed regions in the test plane, θ_{23} versus δ_{13}, at 90% C.I with top, middle, and bottom rows for NOνA runs of $3+\bar{0}$, $3+\bar{1}$, and $3+\bar{3}$ years, respectively.

for 4ν case we see that contour covers the whole of δ_{13} range. Already present small area of RH-WO of 3ν is also increased for 4ν case. 4ν case also introduces a small region of WH solutions which were not present in 3ν case. In the third plot, we see that 4ν introduces RH-WO region of the almost equal size of RH-RO region of 3ν case. We observed a slight increase in WH-RO region for 4ν over 3ν case, while the WH-WO region almost triples for 4ν case.

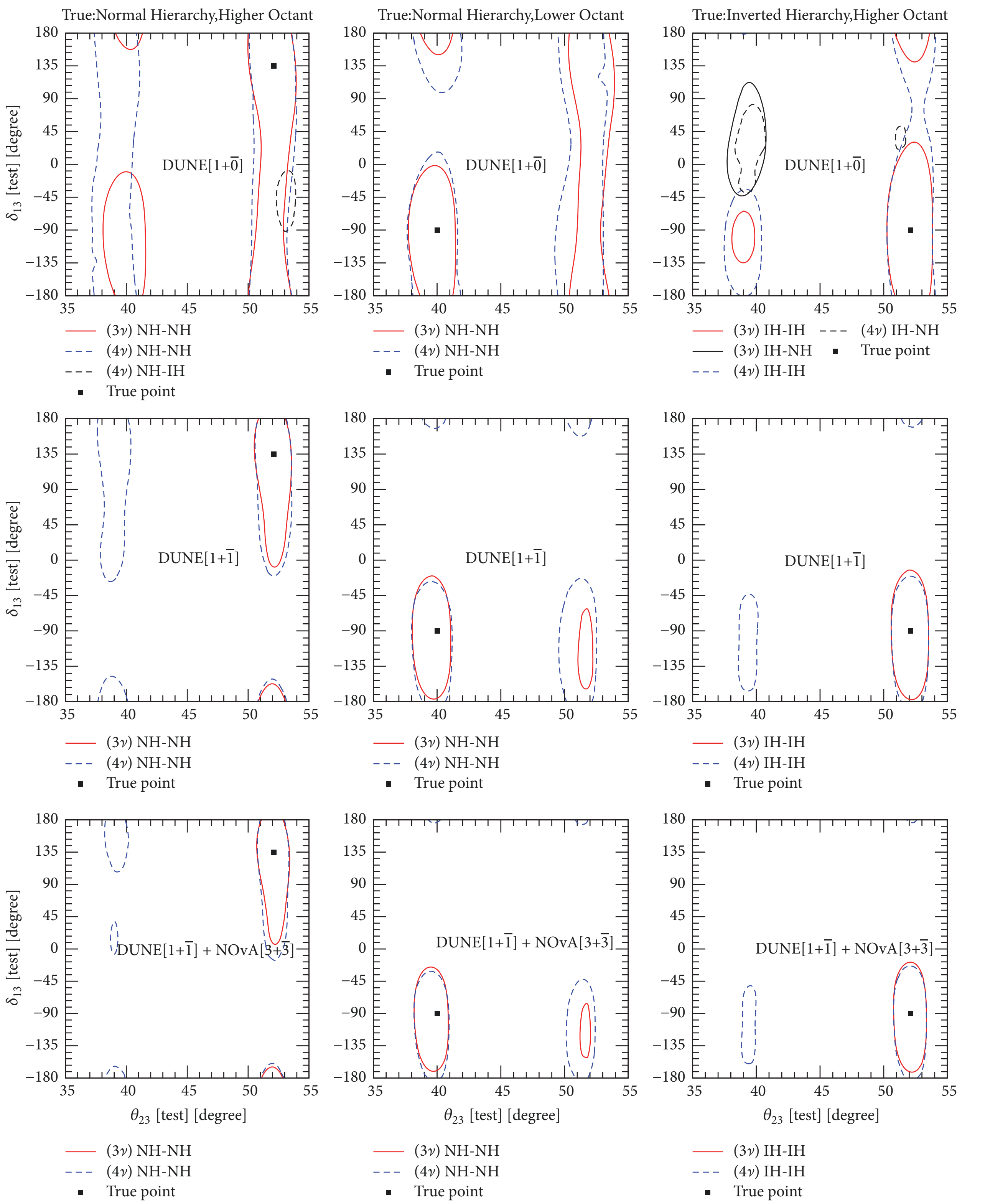

Figure 4: Contour plots of allowed regions in the test plane θ_{23} versus δ_{13} at 99% C.L with top, middle, and bottom rows for DUNE runs of $1+\bar{0}$, $1+\bar{1}$ years and DUNE$[1+\bar{1}]$+NOνA$[3+\bar{3}]$, respectively.

In Figure 4, we show allowed parameter regions for DUNE experiment for different runtimes. DUNE, being the next generation LBL experiment, is expected to have excellent statistics. Hence, we plot 99% C.L regions for DUNE. In the first row of Figure 4, we show 99% C.L for DUNE$[1+\bar{0}]$. In the first plot, RH-RO region covers the entire δ_{13} range for both 3ν and 4ν case. The RH-WO region which covers only lower half of δ_{13} region for 3ν case covers the whole range

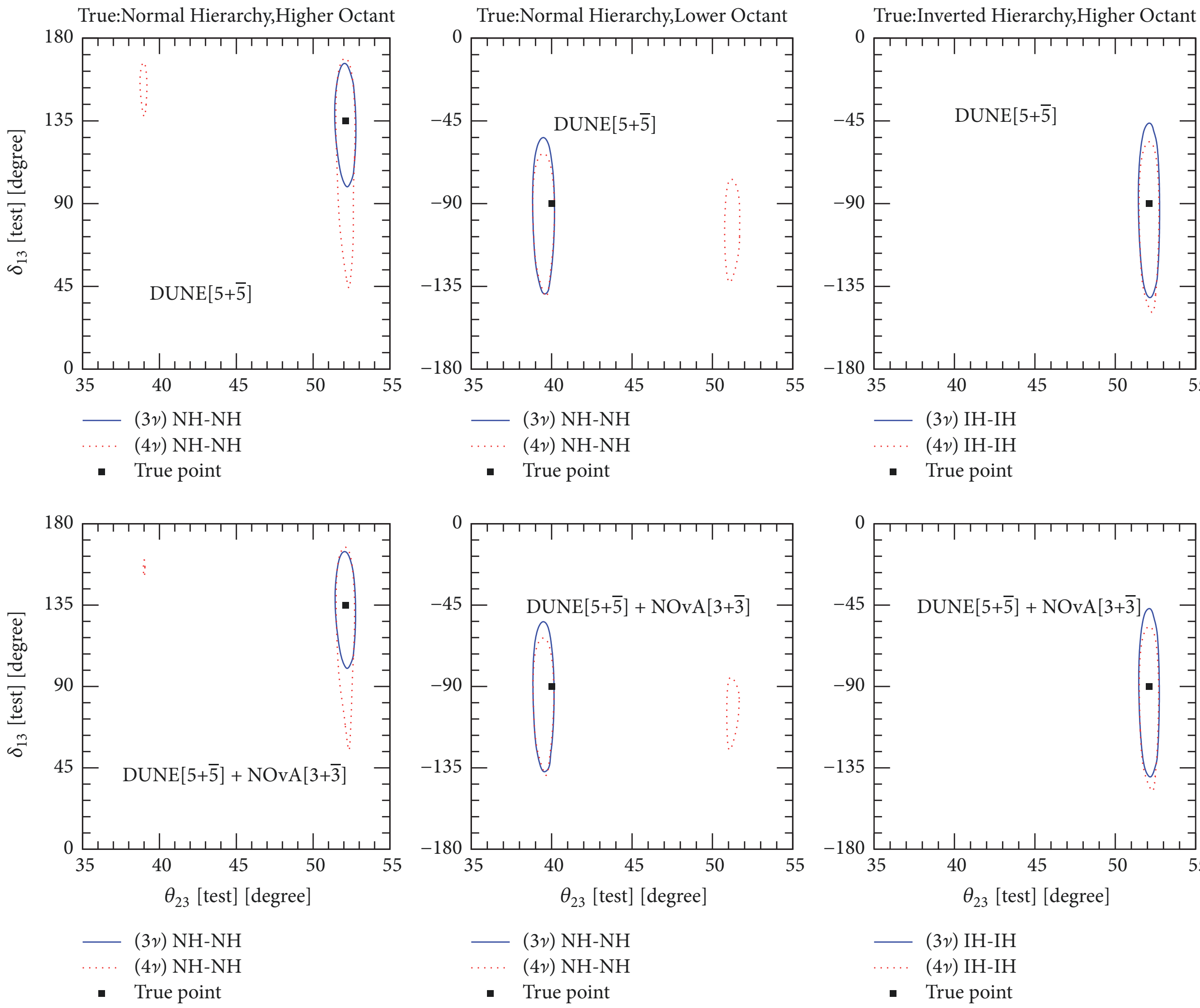

FIGURE 5: Contour plots of allowed regions in the test plane θ_{23} versus δ_{13} at 99% C.L with top and bottom rows for DUNE$[5+\overline{5}]$ and NOνA$[3+\overline{3}]$ + DUNE$[5+\overline{5}]$, respectively.

for 4ν case. A small region of WH is also observed. In the second plot we see that all WH solutions are resolved. RH-WO covers the whole range of δ_{13} for both 3ν and 4ν case. RH-RO solutions exclude 0° to 155° of δ_{13} for 3ν case, while 20° to 100° of δ_{13} are excluded for 4ν case. In third plot, we see that 4ν case extends RH-RO to the whole range of δ_{13} while 30° to 140° of δ_{13} were excluded for 3ν case. We can see that DUNE clearly has better precision than NOνA experiment. In the second row, we show allowed regions for DUNE$[1+\overline{1}]$. We see the WH solutions are resolved for both 3ν and 4ν cases for all the best-fit values. In the first plot, 4ν case introduces RH-WO solution of similar size as RH-RO region of 3ν case. In the second plot, there is no considerable change in 4ν, compared to 3ν case for RH-RO region, while RH-WO octant is approximately doubled for 4ν case compared to 3ν case. In the third plot, 4ν case introduces small region of RH-WO which covers -45° to -170° of δ_{13}. In the third row, we combine statistics of DUNE$[1+\overline{1}]$ and NOνA$[3+\overline{3}]$. There is a small improvement in precision from the combined result over the result from DUNE$[1+\overline{1}]$ alone. In the first plot, we see that a small RH-WO region is introduced by 4ν case. In the second plot, there is no considerable change between 3ν and 4ν case for RH-RO region, while RH-WO octant almost doubles over 3ν case for 4ν case. In the third plot, 4ν case introduces small region of RH-WO which covers -35° to -160° of δ_{13}.

In Figure 5, we show allowed parameter regions for DUNE experiment, at 99% C.L for DUNE$[5+\overline{5}]$. We see that WH regions completely disappear for all the true value assumptions. In the first plot, RH-RO region covers a small δ_{13} range for both 3ν and 4ν case indicating high precision measurement capacity of DUNE. We see that δ_{13} range for 4ν case is approximately doubled as compared to the 3ν case. A small region of RH-WO is observed for 4ν case. In the second plot, RH-RO region covers small δ_{13} range of equal area for both 3ν and 4ν case. A small region of RH-WO is observed for 4ν case. In the third plot, the RH-WO solution is resolved. There is an increase in precision due to an increase in statistics. DUNE$[5+\overline{5}]$ clearly has a better precision compared to the NOνA$[3+\overline{3}]$ experiment. In the second row, we combine full run of NOνA and DUNE to check their degeneracy resolution capacity. The WH solutions are resolved for both 3ν and 4ν cases for all the best-fit values. In the first plot, RH-WO solution is almost resolved for 4ν case. In the second plot, RH-RO region covers small δ_{13} range of equal area for both 3ν and 4ν case. A small region of RH-WO is observed for 4ν case. We observe a slight improvement in degeneracy resolution, on consideration of combined statistics of full run DUNE and NOνA, over DUNE[5+$\overline{5}$].

5. Conclusions

We have discussed how the presence of a sterile neutrino will affect the physics potential of the proposed experiment DUNE and future runs of NOνA, in the light of latest NOνA results [35]. The best-fit parameters reported by NOνA still contain degenerate solutions. We attempt to see the extent to which these degeneracies could be resolved in future runs for the 3+1 model. Latest NOνA best-fit values are taken as our true values. First, we show the degeneracy resolution capacity, for future runs of NOνA. We conclude that NOνA[3+$\overline{3}$] could resolve WH-WO solutions for first two true value cases, at 90% C.L for 3ν case, but not for 4ν case. DUNE[1+$\overline{1}$] could resolve WH and RH-Wδ_{cp} solutions for both 3ν and 4ν case. WO degeneracy is resolved for 3ν case at 99% C.L except for small RH-WO region for the second case of true values. DUNE[1+$\overline{1}$] combined with NOνA[3+$\overline{3}$] shows increased sensitivity towards degeneracy resolution. Finally, for the full planned run of DUNE[5+$\overline{5}$], all the degeneracies are resolved at 99% C.L for 3ν case while a tiny region of WO lingers on for 4ν case. For combined statistics of DUNE[5+$\overline{5}$] and NOνA[3+$\overline{3}$], we observe that all the degeneracies are resolved at 99% C.L for both 3ν and 4ν case except for the NH-LO case. Thus, we conclude that NOνA and DUNE experiments together can resolve all the degeneracies at 99% C.L even in the presence of sterile neutrino, if one of the current best-fit values of NOνA is the true value.

Data Availability

The data used to support the findings of this study are based on published data and licensed open access software.

Conflicts of Interest

The authors declare that they have no conflicts of interest.

Acknowledgments

Akshay Chatla would like to thank *the Council of Scientific & Industrial Research, Government of India*, for financial support. The work of Sahithi Rudrabhatla was supported by *theDepartment of Science & Technology, Government of India*. We would like to thank Dr. Monojit Ghosh, Dr. C Soumya, and K Siva Prasad for their valuable help.

References

[1] R. R. Volkas, "Introduction to sterile neutrinos," *Progress in Particle and Nuclear Physics*, vol. 48, no. 1, pp. 161–174, 2002.

[2] C. Athanassopoulos et al., "Candidate events in a search for $\overline{\upsilon}_{\mu} \longrightarrow \overline{\upsilon}_{e}$ oscillations," *Physical Review Letters*, vol. 75, p. 2650, 1995.

[3] S. Schael et al., "ALEPH and DELPHI and L3 and OPAL and SLD collaborations and LEP electroweak working group and SLD electroweak group and SLD heavy flavour group," *Physics Reports*, vol. 427, p. 257, 2006.

[4] A. A. Aguilar-Arevalo et al., "MiniBooNE collaboration," *Physical Review Letters*, vol. 102, Article ID 101802, 2009, arXiv:0812.2243.

[5] J. N. Abdurashitov et al., "Measurement of the response of a Ga solar neutrino experiment to neutrinos from an 37Ar source," *Physical Review C: Nuclear Physics*, vol. 73, Article ID 045805, 2006.

[6] M. A. Acero, C. Giunti, and M. Laveder, "Limits on υ_e and $\overline{\upsilon}_e$ disappearance from Gallium and reactor experiments," *Physical Review D: Particles, Fields, Gravitation and Cosmology*, vol. 78, no. 7, 2008.

[7] C. Giunti and M. Laveder, "Statistical significance of the gallium anomaly," *Physical Review C: Covering Nuclear Physics*, vol. 83, no. 6, p. 065504, 2011.

[8] G. Mention, M. Fechner, T. Lasserre et al., "Reactor antineutrino anomaly," *Physical Review D: Particles, Fields, Gravitation and Cosmology*, vol. 83, no. 7, Article ID 073006, 2011.

[9] N. Klop and A. Palazzo, "Imprints of *CP* violation induced by sterile neutrinos in T2K data," *Physical Review D: Particles, Fields, Gravitation and Cosmology*, vol. 91, no. 7, 2015.

[10] A. Palazzo, "3-flavor and 4-flavor implications of the latest T2K and NOνA electron (anti-)neutrino appearance results," *Physics Letters B*, vol. 757, p. 142, 2016.

[11] F. P. An et al., "Independent measurement of the neutrino mixing angle θ_{13} via neutron capture on hydrogen at Daya Bay," *Physical Review Letters*, vol. 90, no. 7, 2014.

[12] C. Soumya and R. Mohanta, "Towards extracting the best possible results from NOvA," *European Physical Journal C*, vol. 76, no. 6, p. 302, 2016, arXiv:1605.00523.

[13] C. Soumya, K. N. Deepthi, and R. Mohanta, "A Comprehensive Study of the Discovery Potential of NOνA, T2K, and T2HK Experiments," *Advances in High Energy Physics*, vol. 2016, Article ID 9139402, 15 pages, 2016.

[14] K. N. Deepthi, C. Soumya, and R. Mohanta, "Revisiting the sensitivity studies for leptonic CPviolation and mass hierarchy with T2K, NOνA and LBNE experiments," *New Journal of Physics*, vol. 17, no. 2, Article ID 023035, 2015, arXiv:1409.2343.

[15] M. Ghosh, P. Ghoshal, S. Goswami, N. Nath, and S. K. Raut, "New look at the degeneracies in the neutrino oscillation parameters, and their resolution by T2K, NOνA and ICAL," *Physical Review D: Particles, Fields, Gravitation and Cosmology*, vol. 93, no. 1, Article ID 013013, 2016.

[16] S. Goswami and N. Nath, "Implications of the latest NOνA results," *High Energy Physics - Phenomenology*, 2017, arXiv:1705.01274.

[17] J. Kopp, P. A. Machado, M. Maltoni, and T. Schwetz, "Sterile neutrino oscillations: the global picture," *High Energy Physics - Phenomenology*, vol. 1305, p. 050009, 2013.

[18] M. Ghosh, S. Gupta, Z. M. Matthews, P. Sharma, and A. G. Williams, "Study of parameter degeneracy and hierarchy

sensitivity of NOνA in presence of sterile neutrino," *Physical Review D: Particles, Fields, Gravitation and Cosmology*, vol. 96, no. 7, 2017.

[19] S. K. Agarwalla, S. S. Chatterjee, and A. Palazzo, "Physics reach of DUNE with a light sterile neutrino," *High Energy Physics - Phenomenology*, vol. 016, 2016, arXiv:1603.03759.

[20] D. Dutta, R. Gandhi, B. Kayser, M. Masud, and S. Prakash, "Capabilities of long-baseline experiments in the presence of a sterile neutrino," *Journal of High Energy Physics*, vol. 122, 2016.

[21] S. K. Agarwalla, S. S. Chatterjee, and A. Palazzo, "Signatures of a light sterile neutrino in T2HK," *High Energy Physics - Phenomenology*, vol. 1804, no. 091, 2018, arXiv:1801.04855.

[22] S. K. Agarwalla, S. S. Chatterjee, and A. Palazzo, "Octant of θ_{23} in danger with a light sterile neutrino," *Physical Review Letters*, vol. 118, no. 3, 2017.

[23] S. Choubey, D. Dutta, and D. Pramanik, "Measuring the sterile neutrino CP phase at DUNE and T2HK," *The European Physical Journal C*, vol. 78, no. 4, 2018.

[24] P. Huber, M. Lindner, and W. Winter, "Simulation of long-baseline neutrino oscillation experiments with GLoBES: (General Long Baseline Experiment Simulator)," *Computer Physics Communications*, vol. 167, no. 3, pp. 195–202, 2005.

[25] P. Huber, J. Kopp, M. Lindner, M. Rolinec, and W. Winter, "New features in the simulation of neutrino oscillation experiments with GLoBES 3.0. (General Long Baseline Experiment Simulator)," *Computer Physics Communications*, vol. 177, p. 432, 2007.

[26] J. Kopp, "New physics engine for the inclusion sterile neutrinos and non-standard interactions in GLoBES," https://www.mpi-hd.mpg.de/personalhomes/globes/tools.html, 2011.

[27] P. Adamson et al., "First measurement of muon-neutrino disappearance in NOvA," *Physical Review Letters D*, vol. 93, no. 5, 2016.

[28] P. Adamson, "First Measurement of Electron Neutrino Appearance in NOvA," *Physical Review Letters*, vol. 116, no. 5, 2016.

[29] D. S. Ayres et al., "The NOvA technical design report," *INIS*, vol. 39, no. 38, 2007, [NOvA Collaboration], doi:10.2172/, doi.

[30] S. K. Agarwalla, S. Prakash, S. K. Raut, and S. U. Sankar, "Potential of optimized NOvA for large theta(13) & combined performance with a LArTPC & T2K," *High Energy Physics - Phenomenology*, vol. 1212, 2012, arXiv:1208.3644.

[31] D. S. Ayres et al., "NOvA proposal to build a 30 kiloton Off-axis detector to study neutrino oscillations in the fermilab NuMI beamline," *High Energy Physics - Experiment*, 2005.

[32] R. Acciarri, "Long-baseline neutrino facility (LBNF) and deep underground neutrino experiment (DUNE) conceptual design report volume 2: The physics program for DUNE at LBNF," *High Energy Physics - Experiment*, 2016, arXiv:1512.06148.

[33] R. Acciarri et al., "Long-baseline neutrino facility (LBNF) and deep underground neutrino experiment (DUNE) conceptual design report volume 1: The LBNF and DUNE projects," *High Energy Physics - Experiment*, 2016, arXiv:1601.05471.

[34] T. Alion et al., "Experiment simulation configurations used in DUNE CDR," *High Energy Physics - Phenomenology*, 2016, arXiv:1606.09550.

[35] P. Adamson et al., "Constraints on Oscillation Parameters from υ_e appearance and υ_μ disappearance in NOvA," *Physical Review Letters*, vol. 118, 2017.

[36] P. Adamson et al., "Search for active-sterile neutrino mixing using neutral-current interactions in NOvA," *Physical Review Letters*, vol. 96, no. 7, Article ID 072006, 2017.

[37] A. Y. Smirnov, "The MSW effect and matter effects in neutrino oscillations," *Physica Scripta*, vol. T121, pp. 57–64, 2005.